

# An Automatic Personalized Internal Fixation Plate Modeling Framework for Minimally Invasive Curved Bone Fracture Surgery Based on Preregistration With Capsule Projection Model

Bin Liu , Song Zhang , Yiqian Yang , Mingzhe Wang , Xiaohui Zhang , Jianxin Zhang , Wen Qi , and Liang Yang 

**Abstract—Objective:** In this paper, a framework to visualize and model internal fixation plates is presented for computer-aided personalized and minimally invasive curved bone fracture surgery. **Methods:** We focus on personalized reverse reconstruction of the bone fracture plate based on three-dimensional (3-D) mesh models obtained from a 3-D optical scanner. The steps of the method are as follows. First, principal component analysis and the K-means method are used to reconstruct a Bezier curve (ridge line) of broken bones. Second, based on the geometric shape of the curved broken bones, a capsule projection model of the broken bones is proposed to obtain the feature information of the broken bone sections. Third, the ordering points to identify the clustering structure (OPTICS) method is utilized for preregistration (rough registration). Fourth, a regional self-growth strategy is designed to extract the cross-section points. Fifth, the iterative closest point method is applied for the accurate registration of the fracture surface models. Finally, a personalized internal fixation plate model is reconstructed based on several user points. **Results:** The internal fixation plate model can be reconstructed according to the patient's bone parameters.

Manuscript received April 17, 2019; revised May 9, 2019 and May 15, 2019; accepted May 26, 2019. Date of publication May 30, 2019; date of current version February 19, 2020. This work was supported in part by the National Natural Science Foundation of China under Grants 61572101 and 61300085, in part by the National Key Research and Development Program of China under Grant 2016YFB1101100, and in part by the Scientific Research Fund of the Liaoning Provincial Education Department of China under Grant L2013012. (Corresponding author: Liang Yang.)

B. Liu is with the International School of Information Science & Engineering (DUT-RUISE), and the Key Lab of Ubiquitous Network and Service Software of Liaoning Province, Dalian University of Technology.

S. Zhang, Y. Yang, M. Wang, and X. Zhang are with the International School of Information Science & Engineering, Dalian University of Technology.

J. Zhang is with the Key Lab of Advanced Design and Intelligent Computing, Ministry of Education, Dalian University.

W. Qi is with the Department of Nursing, Anshan Health School.

L. Yang is with the Second Hospital of Dalian Medical University, Dalian Medical University, Dalian 116044, China (e-mail: yangliang\_dmu@sina.com).

This paper has supplementary downloadable material available at <http://ieeexplore.ieee.org>, provided by the authors.

Digital Object Identifier 10.1109/TBME.2019.2919897

**Conclusion:** Clinicians can use this framework to obtain personalized and accurate internal fixation plate models that effectively represent the broken bones of patients. Via X-ray navigation, the personalized forged plate can be fixed on the target area through a small incision. **Significance:** This framework provides a reasonable and practicable technical approach for computer-aided minimally invasive curved bone fracture surgery.

**Index Terms**—Personalized modeling, capsule projection model, minimally invasive surgery, curved bone fracture.

## I. INTRODUCTION

BONE fractures are common and occur each day around the world. The ultimate goal of fracture treatment is to recover most of the biological function of the injured limb. In the treatment of fractures, fracture reduction and fixation are critical processes. The aim of reduction is to restore the displaced broken bone to the normal state or close to the original anatomical relationship. External fixation refers to broken bones fixed by a small splint, a plaster bandage, an external bracket, a traction brake, etc. Internal fixation refers to broken bones fixed by a surgical steel plate, a screw, etc. Currently, internal fixation treatment is the most common surgical method. In this procedure, the fractured bones are manually aligned by surgeons, and an internal fixation plate is bent according to personal experience (surgeons will select the fixation position, angle, etc., according to subjective consideration of specific injuries) [1], [2]. However, this personal experience-based treatment may lead to poor surgery results. If the surgery fails, serious clinical consequences can occur, such as bone nonunion or malunions, disability, decreased general health, and the need for secondary operations. Such surgeries also have an important influence on the patient's physical and psychological well-being [3]. In actual clinical treatment, to restore the mechanical properties of bones, the most important treatment goal is achieving accurate broken bone alignment and precise internal fixation plate molding. Improving the accuracy of alignment can lead to better recovery of mechanical properties. On this basis, a precise internal fixation plate can promote the healing of broken bones [4]. In

addition, reducing the operation time and avoiding aerial infection are critical. Under these conditions, developing more precise computer-aided surgical methods for bone fractures remains a considerable challenge.

## II. RELATED WORKS

Computer-aided bone fracture planning and surgery is an emerging research issue. Consequently, compared to a large amount research findings about bone segmentation and registration, there are not very many published papers regarding this issue. In this section, we review the existing research works that are most relevant to our research. As a representative work, Jiménez-Delgado *et al.* recently completed a comprehensive survey report [5]. They not only summarized the published approaches for bone fracture planning and surgery but also discussed the challenges and new trends of this open field of research.

Some of the existing methods are based on contralateral bone models or statistical shape models [6]–[10]. For example, Okada *et al.* described a preoperative planning method for femoral fracture reduction [6]. They utilized three constraints (e.g., femur shape) to achieve registration of bone fragments. Albrecht *et al.* proposed a method to automatically reposition the fragments of a broken bone based on surface meshes using a modified iterative closest point (ICP) algorithm [7]. They also suggested to use the same patient's contralateral bone or the statistical shape model as a reference. However, these specific methods are focused on specific bone fractures ([6] focuses on femoral neck fractures; [7] can mainly achieve long straight bone fracture planning), and the fracture surface shapes that can be processed via these methods are different from the fracture surface shape of curved bones (e.g., ribs). In addition, due to physiological structure difference between bones, some studies [11] concluded that we should not rely blindly on the contralateral anatomy. For example, in human body, ribs on the left side generally do not have the same shape with ribs on right side because of thoracic organ asymmetry or skeletal disease [12]–[14]. Furthermore, statistical shape model method may be a suitable choice for rough registration. However, to obtain a final accurate personalized model, relying on a statistical shape model is insufficient.

Some of the existing methods are based on fracture surface characteristics [6], [15]–[17]. For example, Vlachopoulos *et al.* proposed a scale-space representation of the curvature, permitting calculation of the correct alignment between bone fragments solely based on corresponding regions of the fracture lines [15]. This method can achieve an accurate approximation of the pre-traumatic anatomy. We previously designed a computer-aided preoperative planning system for long straight bone fractures [16]. In this method, the principal component analysis (PCA) method is used to extract the three-dimensional (3D) axis of the broken bone. Then, the Gauss mapping method is utilized to segment the end surfaces of the broken bone. However, the extracted characteristics in these methods are not suitable for curved bone fractures. For example, method [15] regards the fracture surface as a curved line. However, the

method is not effective for some solid column curved bones (e.g., ribs). In method [16], the processing strategy is unstable and usually unfeasible for curved bone fractures. Especially in the case of a large-angle cuneate end surface, the Gauss mapping will consider the end surface as the side face of the broken bone. Thus, the end surface of the broken bone cannot be automatically and accurately extracted.

In addition, some prediction-based methods have provided technical assistance regarding bone fractures [18]–[22]. For example, Leslie *et al.* investigated whether repeat bone mineral density (BMD) measurements in clinical populations are useful for fracture risk assessment [21]. They proposed that repeat BMD measurements are a robust predictor of fractures in clinical populations. From the perspective of computer-aided design, Pauchard *et al.* proposed an interactive graph cut method [22]. This method can achieve fast creation of femur finite element (FE) models from clinical computed tomography scans for hip fracture prediction. However, these methods are mainly utilized in reoperation planning for bone fractures and do not provide a detailed strategy of fracture reconstruction (especially for curved bone fractures).

These previous publications indicate that computer-assisted fracture reduction and surgery is an important research topic in clinical medicine. However, for common curved bone (e.g., ribs) fractures, there have been no direct studies regarding computer-assisted preoperative reconstruction. Developing detailed methods for computer-assisted preoperative planning for minimally invasive curved bone fracture treatment has become a new research topic. This paper focuses on this challenging issue.

## III. METHODS

### A. Overview of Our Method Framework

In this paper, we introduce a recently developed computer-assisted preoperative planning system for curved bone fracture surgery. A flow chart of this system is shown in Fig. 1. Specifically, the 'Personalized reverse reconstruction of the bone fracture plate' task is the most pivotal process in the flow chart. Therefore, this paper focuses on this core technology, and an automatic personalized internal fixation plate modeling framework for minimally invasive curved bone fracture surgery is proposed. This modeling framework is applicable for use in curved bone fractures ("Rib, shaft, fracture" with type number "16.1 or 2.1–20.2A" in the AO/OTA Fracture and Dislocation Classification Table).

### B. Broken Bone Curve Fitting

Bone models of multiple broken bones are difficult to directly register. To obtain shape information for broken bone models, the curves of broken bones must be fitted. Here, a curve is the ridge line of a broken bone and is used in the general shape of the broken bone. The Bezier curve is used in this process. However, the number of vertices in original mesh models is very large, and the vertices cannot all be used to fit curves. Therefore, we introduce a clustering method for curve fitting. First, the main axis of the model is extracted using a PCA algorithm (shown

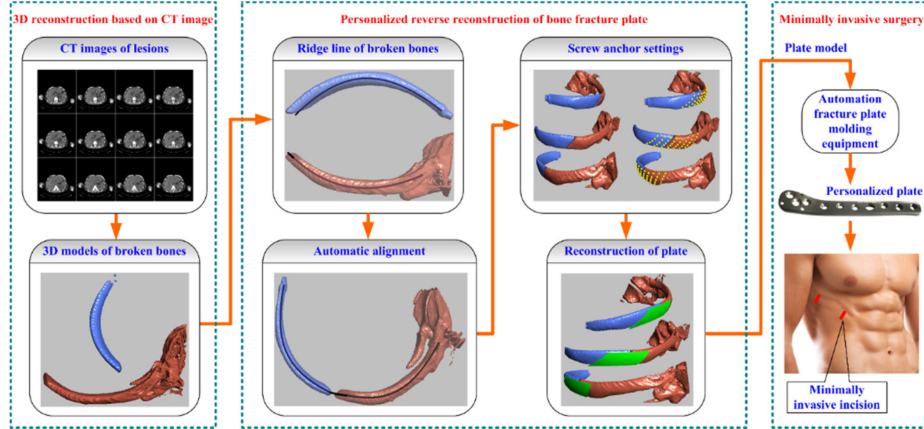


**Fig. 1.** System flowchart of the computer-aided preoperative planning system.

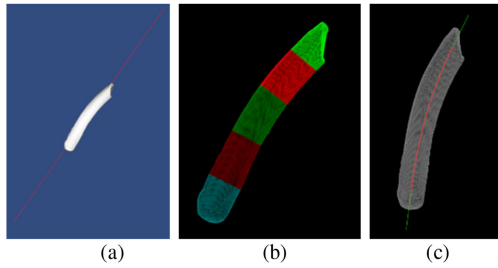


**Fig. 2.** Three steps of curve fitting. (a) Extraction of the main axis of the broken bone model. (b) Cluster result for points in the model. (c) The fitted curve and tangents at the ends of the curve.

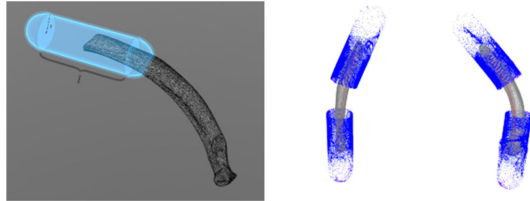


**Fig. 3.** Capsule projection models of broken bones ( $l$  is set to 50 mm and  $r$  is set to 10 mm in this paper).

in Fig. 2(a)). PCA is widely used in feature extraction and dimensionality reduction. The main axis is a straight line that is extracted according to the coordinates of the points based on PCA. Then, 5 seed points are selected along the main axis as the initial center points. (5 is a suitable empirical value for most broken bone models. If a large number of seed points is selected for some broken bone models, the obtained cluster center points will not well represent the shape of the broken bone.) The points in the model are clustered using the K-means algorithm based on their coordinates. The cluster result is shown in Fig. 2(b). Next, the center points of the clusters are calculated. Finally, a Bezier curve can be fitted based on these cluster center points. The formula for an n-order Bezier curve [23] is

$$B(t) = \sum_{i=0}^n C_n^i P_i (1-t)^{n-i} t^i \quad (1)$$

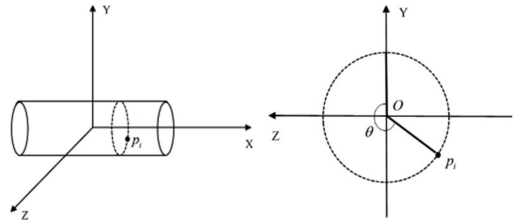


**Fig. 4.** Definition of  $\theta$ . The left subfig. shows the projection point  $p_i$  and the circular section where it is located. The right subfig. shows the definition of  $\theta$  in the circular section.  $O$  is the circle center.  $\theta$  is a positive angle formed by counterclockwise rotation. The starting edge is the positive y-axis, and the ending edge is  $Op_i$ .

where  $C$  is the combinatorial number of the Bezier equation,  $n$  is the order,  $t$  is the parameterized interval with a range of  $[0, 1]$ , and  $P_i$  represents the coordinates of the  $i$ th center point. As shown in Fig. 2(c), the curve of the broken bone model can be fitted by adding the 5 center points to the formula.

### C. Capsule Projection Model Construction for Broken Bones

The broken bones are registered mainly based on the features of cross-sections. For example, the rough registration process relies on the shape information of the section, and the precise registration process relies on the section points of the broken bone model. Therefore, it is important to obtain the feature information (shape, spatial location and point distribution) of the broken bone sections. However, it is difficult to directly obtain the feature information because the shapes of the sections are often complicated. An effective method to obtain this information is to compare the points in two broken bone models and find the sets of points with the highest degree of matching. Therefore, projection models with the same size are needed for the point comparison.

As shown in Fig. 3, for the special geometric shape of curved broken bones, a capsule projection model for broken bones is proposed in this paper. The capsule projection model has a cylinder in the middle and a hemisphere at both ends. We first calculate the tangents at the ends of the curves. The projection

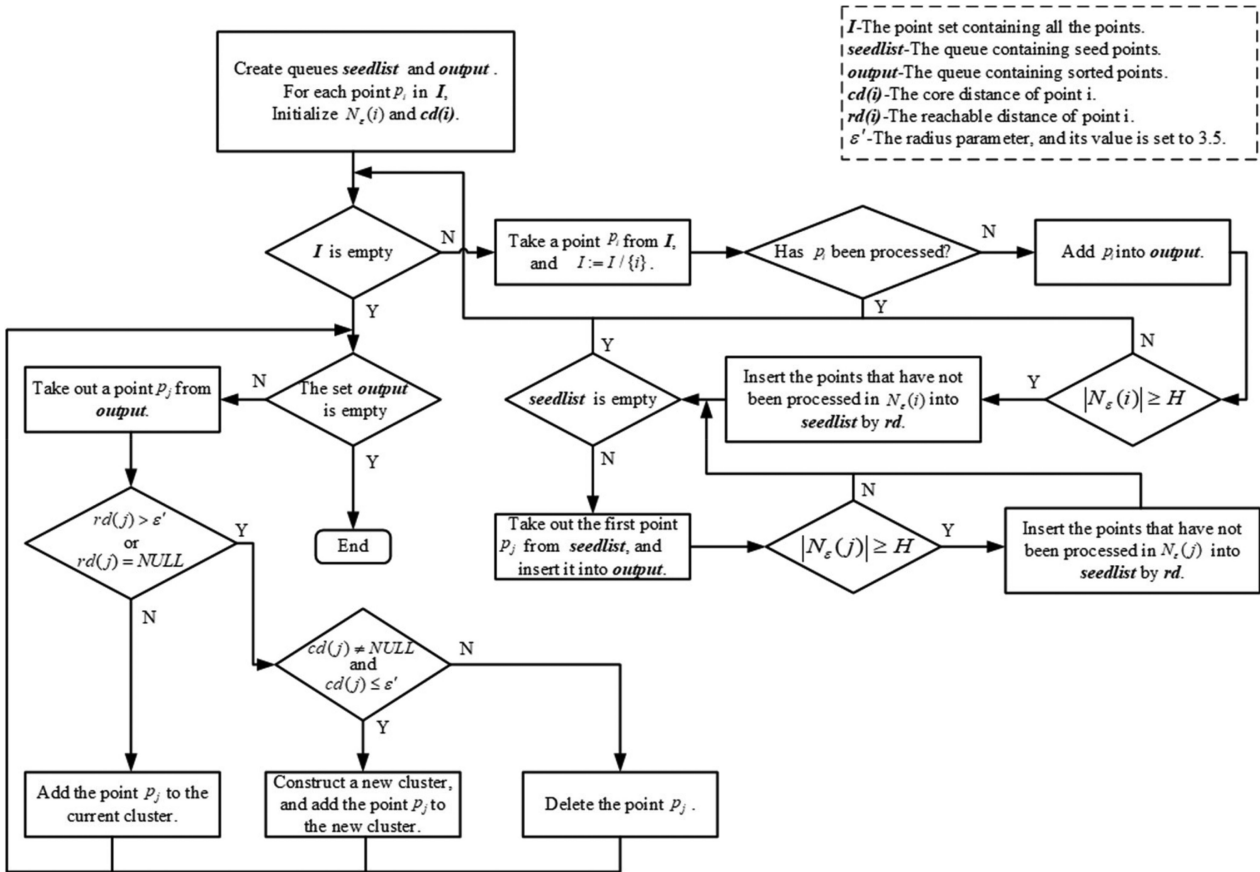


Fig. 5. Flowchart of the clustering process.

model takes the tangent as the axis, and the geometric center is located at the end point of the curve. To facilitate model construction, the tangential direction is set in the increasing  $x$  direction, and the end point of the curve is set as the origin. Suppose the radius of the hemisphere is  $r$  and the length of the cylinder is  $l$ . Therefore, in a Euclidean coordinate system, the projection model can be expressed as follows:

$$\begin{cases} y^2 + z^2 = r^2 & \left( -\frac{l}{2} \leq x \leq \frac{l}{2} \right) \\ \left( x - \frac{l}{2} \right)^2 + y^2 + z^2 = r^2 & \left( x > \frac{l}{2} \right) \\ \left( x + \frac{l}{2} \right)^2 + y^2 + z^2 = r^2 & \left( x < -\frac{l}{2} \right) \end{cases} \quad (2)$$

The points within the range of the projection model (we only consider the points in the range of the cylindrical area and ignore the points in the hemisphere because the goal is to extract the section points) are added to the model with their normal vectors.

#### D. Rough Registration of the Broken Bones

Although the construction of capsule projection models is now complete, the two corresponding models cannot be directly matched. Notably, one model requires a mirror transform. Because the geometric center of the projection model

I - The point set containing all the points.  
Iseedlist - The queue containing seed points.  
Ioutput - The queue containing sorted points.  
cd(i) - The core distance of point i.  
rd(i) - The reachable distance of point i.  
 $\epsilon'$  - The radius parameter, and its value is set to 3.5.

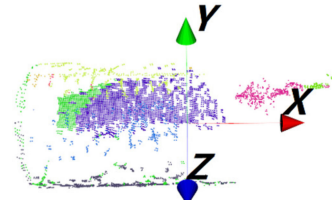


Fig. 6. Clustering result of projection points. In the coordinate system, points with the same color are located in the same cluster. Different colors represent different clusters.

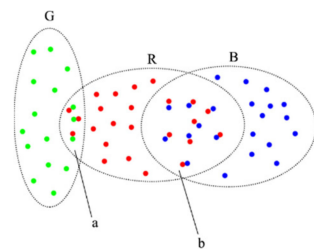


Fig. 7. Registration of projection points. R and B are the two point sets to be registered. G is a point set that also has points that match those in R.

is the origin, we can simply change the  $x$  coordinate of each projection point to the opposite value. However, if the number of projection points is too large, the point set must be simplified. In the projection model, the dense regions are more likely

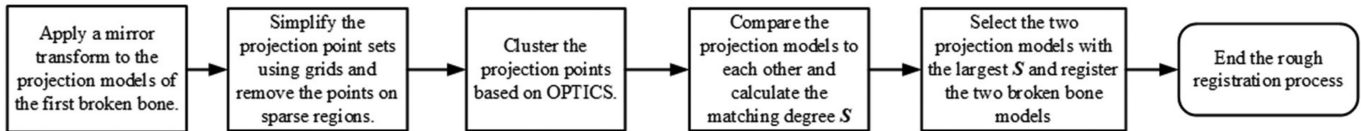


Fig. 8. Flowchart of the rough registration process.

to reflect the features of the section. Therefore, the points in dense regions must be extracted, and the points in sparse regions must be removed. Cube cells are used in this process. The surface of the cylinder is divided into many cube cells. Here, the cylinder represents the central part of the projection model. The length and width of the cylinder surface are divided into  $n_x$  and  $n_y$  (empirical values according to different 3D broken bone models), respectively. Assume that the number of cube cells is  $N_{\text{cubecell}} = n_x \times n_y$ .

For a projection point  $p_i (x_i, y_i, z_i)$ , the index of the cube cell where  $p_i$  is located is  $(\frac{n_x(2x_i+l)}{2l}, \frac{n_y\theta}{2\pi})$ , and  $\theta$  is the positive angle, which is defined based on the circular section where  $p_i$  is located. Fig. 4 shows the definition of  $\theta$ , which takes the positive y-axis as the starting edge. Now, the number of points in each cube cell can be counted. If the number of points in a cube cell is less than  $\delta$  ( $\delta$  is a threshold and is set to an empirical value of 3 in this paper according to the specific 3D broken bone models), the points will be removed from the projection point set. After the points are simplified, the features of the broken bone sections are more obvious. Next, the projection points are clustered based on density. The Ordering Points to Identify the Clustering Structure (OPTICS) algorithm [24] is applied in this process. OPTICS is a density-based clustering method and is adaptive to different densities. First, the core distance of  $p_i$  is defined as

$$cd(i) = \begin{cases} \text{NULL} & |N_\varepsilon(i)| < H \\ d(x, N_\varepsilon^H(i)) & |N_\varepsilon(i)| \geq H \end{cases} \quad (3)$$

where  $N_\varepsilon(i)$  is a point set containing the points within radius  $\varepsilon$  of  $p_i$  ( $\varepsilon$  is a parameter that is set to 4.5 in this paper according to the specific 3D broken bone models).  $N_\varepsilon^H(i)$  is the  $H_{th}$  closest point to  $p_i$  ( $H$  is set to 5 in this paper according to the specific 3D broken bone models).

The reach distance from  $p_i$  to  $p_x$  is defined as follows:

$$rd(i, x) = \begin{cases} \text{NULL} & |N_\varepsilon(x)| < H \\ \max\{cd(x), d(x, i)\} & |N_\varepsilon(x)| \geq H \end{cases} \quad (4)$$

The main clustering process is shown in Fig. 5. As shown in Fig. 6, the projection points form several clusters after clustering. Next, the center points of clusters are extracted, and the clusters are registered by matching the center points. For center point  $q_i$ , assume that the associated positive angle is  $\theta_{q_i}$ . When a cluster center point matches another point, the corresponding  $\theta_{q_i}$  values are set by rotating the projection model around its axis until they are equal.

There are 4 projection models in total. In the process of rough registration, they are compared, and the degree of matching is calculated. When comparing the two projection models  $M$  and  $M'$ , the clusters  $C_i$  and  $C'_j$  in the two models are evaluated.

First, the two clusters are registered by matching the center points. Then, for each projection point  $p'_j$  in the model  $M'$ , the closest point  $p_i$  in the model  $M$  is identified. Finally, the matching degree  $S$  is calculated. The registration process is shown in a schematic diagram in Fig. 7. Suppose that R and B are the two point sets to be registered. G is a point set that also has points that match those in R. Suppose that collection a is the matching point set of G and R and that collection b is the matching point set of B and R. The matching degree of R and B can be calculated as follows:

$$S = \begin{cases} \frac{n}{m} + \frac{m}{N} + \frac{\min(N, N')}{\max(N, N')} & m + m' \geq 2000 \\ 0 & m + m' < 2000 \end{cases} \quad (5)$$

where  $n$  is the number of points in collection b and  $m$  is the total number of points in collections a and b. This value represents the number of all matching points in R.  $N$  indicates the total number of points in R.  $m'$  and  $N'$  are defined for point set B and have the same meaning as  $m$  and  $N$ ; 2000 is an empirical value. Equation (5) is used to measure the matching degree of two clusters, which is a statistics-based measuring method. When the number of points is small, the error will be large. In addition, clusters with a small number of points are often formed by noise points. Therefore, this threshold is utilized to filter out useless clusters. Clusters with more than 2000 points will be considered, and clusters with fewer than 2000 points will be eliminated. This process will not only increase the matching efficiency but also decrease the error.

Next, the rough registration is implemented. The main steps include the mirror transform for broken bones, projection point simplification, projection point clustering, matching degree calculation and broken bone pair registration. The clusters in the 4 projection models are compared, and  $S$  is calculated for each pair. The pair of clusters with the largest  $S$  comprises the projection point set of the broken bone section. The relevant point sets are extracted, and the broken bone model is rotated to register the point sets. The flow chart of the rough registration process is shown in Fig. 8, and the results are shown in Fig. 9.

### E. Extraction of the Point Set From Broken Bone Cross-Sections

To achieve registration of fractured bones, an existing method is based on fracture lines as described in [6]. However, this method absolutely relies on the integrality of fracture lines. If some tissue loss occurs on the fracture surface, the extracted fracture lines will be inaccurate. Consequently, the registration result will also be inaccurate, and malposition will easily occur. In contrast, the integrality of the fracture surface point cloud and the distribution of points have little effect on the

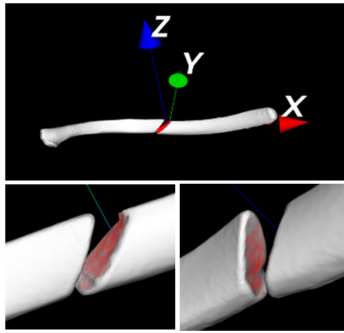


**Fig. 9.** Rough registration of a broken bone model. Model points corresponding to the matching projection points are marked in red.

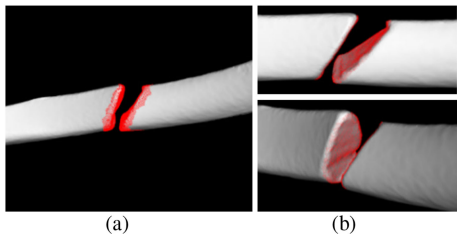


**Fig. 10.** Extraction of cross-section points. (a) Result of regional self-growth. (b) Extracted cross-section points.

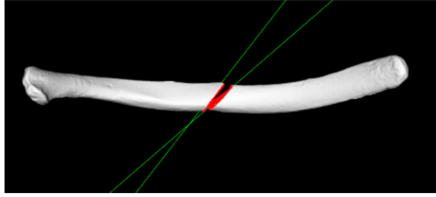


**Fig. 11.** Preregistration of two broken bone models.

registration results. Even if the extracted fracture surface point cloud is not very holonomic, the registration results will also be acceptable. Therefore, the fracture surface point cloud-based method has probably higher accuracy and robustness than the fracture line based method. In our opinion, point cloud-based method should be priority selection. Thus, in our method, to precisely register the broken bones, the point sets from the broken bone cross-sections should be extracted.

In the previous step, the two clusters  $C$  and  $C'$  are extracted, and the two broken bone models are registered. In this step, the model points corresponding to the projection points in  $C$  and  $C'$  are first extracted. A regional self-growth method is applied to the extracted model points to form two point sets  $R$  and  $R'$ , as shown in Fig. 10(a). In this process, the model points projecting in the hemisphere region are also considered part of the broken bone cross-section and are also utilized as seed points for cross-section extraction. For the points projecting in the hemisphere region, the included angles between their normal vectors and the tangent line of the fitted curve are small. Although the point set of the cross-sections is obtained by the previous process, some useful points may be missed because of

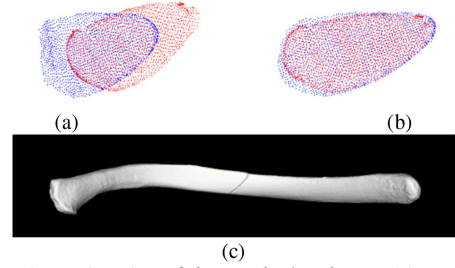


**Fig. 12.** Precise registration of the two broken bones. (a) Locations of the two cross-section point sets before precise registration. (b) Registration results of the two point sets. (c) Registration results of the two broken bone models.

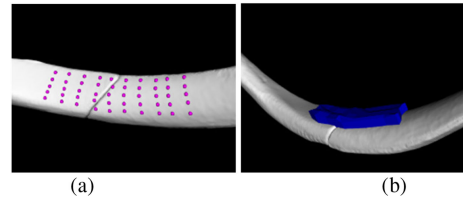


**Fig. 13.** Construction of the plate model. (a) Selection of control points. (b) Plate model fitted based on the control points.



**Fig. 14.** 3-D scanner used to collect the 3-D model of ribs.

the projection and clustering procedure. Therefore, according to the obtained point set, the regional self-growth method is utilized to further extract a more accurate cross-section point set. This process will improve the accuracy of the subsequent registration. Then, the two point sets are traversed to find the matching cross-section points. Suppose that  $p = (x_p, y_p, z_p)^T$  and  $p' = (x'_p, y'_p, z'_p)^T$  are two matching points that satisfy the following condition:

$$\|p - p'\|_2 < \varepsilon_1 \quad (6)$$

After the rough registration process, the two broken bone cross-sections are similar. Therefore, if the two points match, the distance between them should be small. If  $\varepsilon_1$  is set to be too large, the distant non-cross-section points will be introduced. If  $\varepsilon_1$  is set to be too small, some cross-section points will be missed. After many experiments, we found that  $\varepsilon_1 = 4.5$  generates the best effect.

$$\|v + v'\|_2 < \varepsilon_2 \quad (7)$$

$v$  and  $v'$  are unit normal vectors at the two points. For two matching points in the models, the corresponding normal vectors typically have the opposite direction.  $\varepsilon_2$  is utilized to limit the

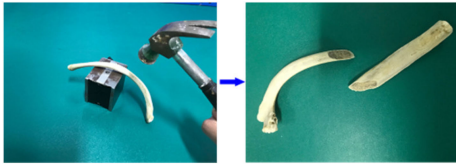


**Fig. 15.** Ribs were manually fractured with a hammer.

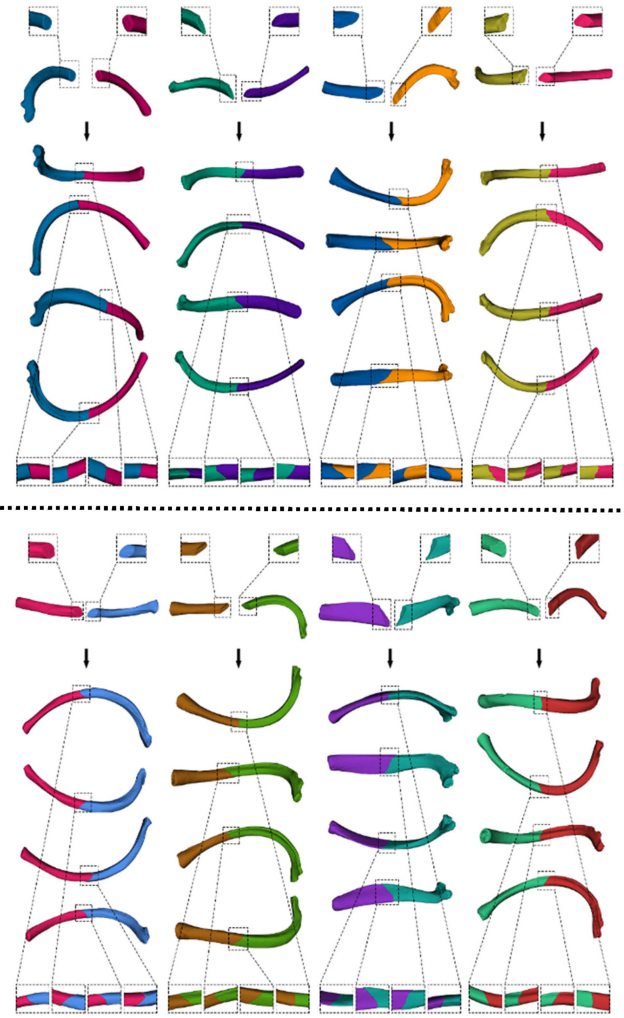


**Fig. 16.** Results of visual validation. Broken bones with different cross-sections are registered. The corresponding sections are all closely pieced together.

included angle between the normal vectors of two matching points. After many experiments, we found that  $\varepsilon_2 = 1.0$  will generate the best effect.

The cross-section points are extracted from  $R$  and  $R'$  according to the former conditions. The result is shown in Fig. 10(b).

## *F. Precise Registration of the Broken Bones*

There is often a considerable error associated with rough registration, and thus, precise registration is needed to accurately register broken bones. Precise registration is based on the cross-section points extracted in the previous step. To further reduce

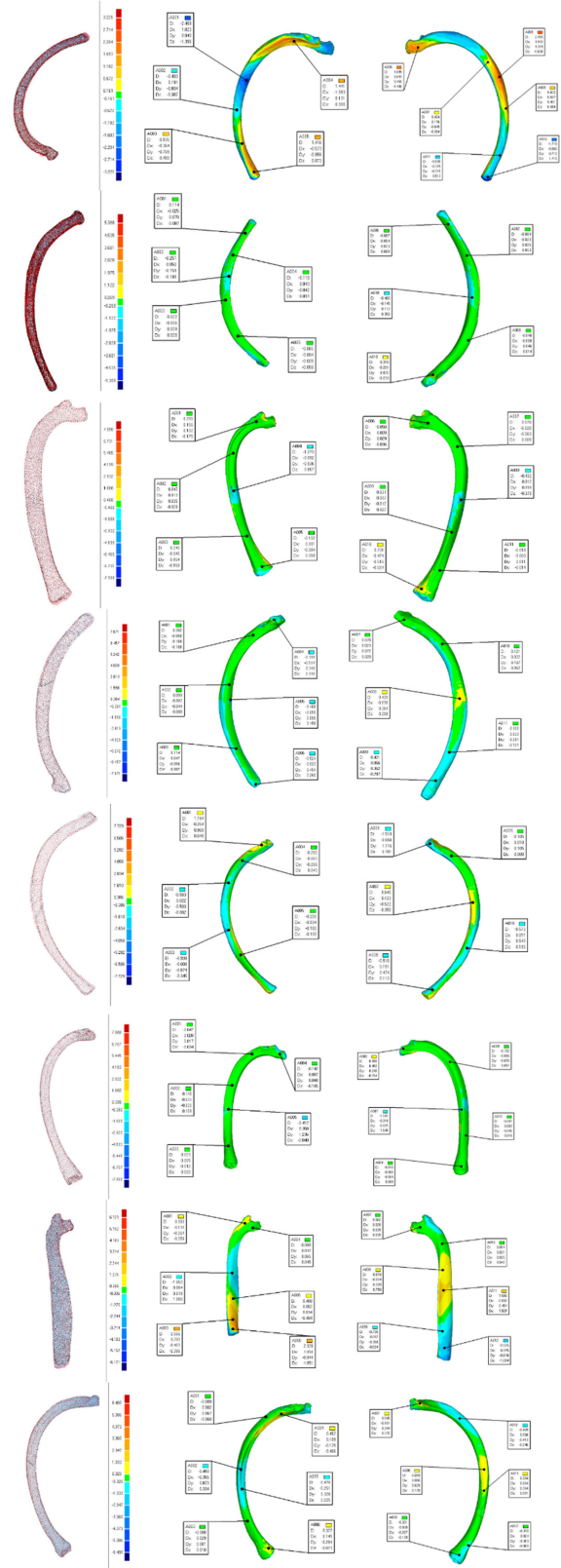


**Fig. 17.** Results of the computational validation. The error between the models before fracture and after registration was computed. Different colors represent different error values. In Geomagic Qualify, the models before fracture formation were used as references, and the registered models were tested. Thus, the obtained distance is a vector with both positive value and negative value.

the error, the cross-section points are first preregistered. The main directions of the two point sets are calculated using the PCA algorithm. Then, the two direction vectors are aligned. As shown in Fig. 11, the two cross-sections are further registered based on their main directions. Based on the preregistration results, the cross-section points can be precisely registered using the ICP algorithm, which is a classic algorithm for point set registration that is reliable and highly convergent [25]. In our method, the error metric for ICP (under point-to-point metric) is as follows: the number of iterations is 200, and the iterative termination distance is  $10^{-5}$ . In Fig. 12, the two cross-section point sets are accurately registered. Therefore, the two broken bone models are accurately registered through the previous steps. Our method is insensitive to the source model and target model order. If the source model and target model are switched (also under point-to-point metric), the difference between the two registration modes is minor (average difference: about 0.02 mm) and both are acceptable for clinical applications.

#### G. Plate Modeling of a Broken Bone

Based on the registration of the two broken bone models, the plate model can be automatically fitted using the surface fitting algorithm. Before fitting, control points around the location of the bone fracture are selected (shown in Fig. 13(a)). In our framework, the control points are manually selected. The control point matrix is  $5 \times 10$ . For the selection means of control points, many factors are considered. The most important factor is the surgical factor. In clinical treatment, the location of the internal fixed steel plate is based on several factors, such as surgical approach and organ occlusion. Surgeons often decide the location of internal fixed steel plates based on their experience.

Then, a smooth surface can be fitted using the NURBS [26] algorithm (the corresponding weights of all the control points are 1) based on the control points. This surface is the inner surface of the plate model. For convenient observation and 3D printing, the final plate model is constructed by thickening the surface along the normal vectors. Fig. 13(b) shows the constructed plate model. As the use of rapid-prototyping technology (3D printing) for the generation of patient-specific instruments is well accepted in orthopedic surgery [6], [27]–[29], our obtained plate model can be directly utilized as the data source of a 3D printing system.

If creation of a plate with minimal contact area with the bone surface (for example, LC-DCP plates) is required, our framework can also generate the spatial geometrical data of the contact area.

## IV. EVALUATION AND RESULTS

To verify the accuracy and robustness of the proposed method, three experiments (visual validation, computational validation, and 3D printing validation) were performed. In the experiments, 8 real ribs of sheep were utilized.

Completely intact sheep ribs were obtained for the experiments. For comparison with the models after registration, the

3D models of the original intact ribs must be initially obtained. As shown in Fig. 14, an object 3D scanner (manufacturer and model: WIIBOOX REEYEE) was used to obtain 3D models of the intact ribs. Then, the ribs were manually fractured with a hammer, as shown in Fig. 15, and 3D models of the broken bone models were also obtained using the 3D scanner. Finally, the method proposed in this paper was applied to the broken models, and the registered models and virtual plates were obtained.

#### A. Visual Validation

We want to validate the feasibility of our framework from coarse to fine perspectives. For coarse, visual validation, we assess whether our framework can achieve the splicing of broken bones and whether there are obvious geometrical discrepancies. In this experiment, the registered bones were verified by visual observation. As shown in Fig. 16, the 8 ribs with different cross-sections were all successfully spliced, and no obvious geometrical errors were observed.

Based on these visual observations, the basic feasibility of our framework can be proven.

#### B. Computational Validation

To further verify the accuracy of registration, a computational validation experiment was conducted. In this validation, the models before fracture formation were used as references, and the registered models were tested. For each group, the error of registration was computed according to the difference between the two models. In this process, geometrical analysis software (Geomagic Qualify, version 11) was utilized to achieve registration of the intact and spliced models and to compute the geometrical errors. As shown in Fig. 17, the model before fracture formation and the model after registration were nested. Then, the error value between the two models was computed and expressed in different colors.

The computational validation results show that the registration method accurately restored the intact ribs, and the geometric error was small (between  $\pm 2.6$  mm). The detailed statistical results of the accuracy (in absolute value form) are reported in Table I. In some groups, the geometric error is slightly larger at seams because some small rib tissue may be lost in the manual fracture process.

#### C. 3D Printing Validation

The goal of this study is to automatically and precisely construct a plate based on broken bone models. Therefore, the most intuitive method for validation is to develop a plate based on the virtual plate model and test the bonding effect. Because the required forging equipment was not available, 3D printed plates were used to simulate real steel plates. As shown in Fig. 18, a 3D printer (manufacturer and model: Myriwell RL200A; printing resolution: 0.15 mm) was used to print plates based on the virtual plate models.

**TABLE I**  
STATISTICAL RESULTS OF THE ACCURACY (IN ABSOLUTE VALUE FORM)

Index Error (mm)	Model_1	Model_2	Model_3	Model_4	Model_5	Model_6	Model_7	Model_8
Mean error	0.774	0.146	0.379	0.305	0.569	0.218	1.003	0.250
Std. error	0.897	0.310	0.790	0.541	0.819	0.554	1.821	0.364
Maximum error	2.493	0.400	1.273	0.524	1.510	2.412	2.566	0.659
Minimum error	0.034	0.004	0.001	0.002	0.002	0.003	0.019	0.008

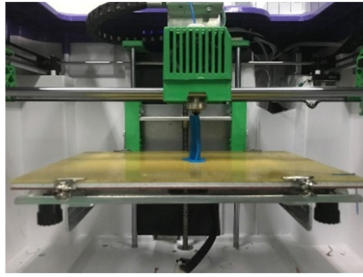


**Fig. 18.** 3-D printer was used to manufacture the plates based on the fitted plate models.

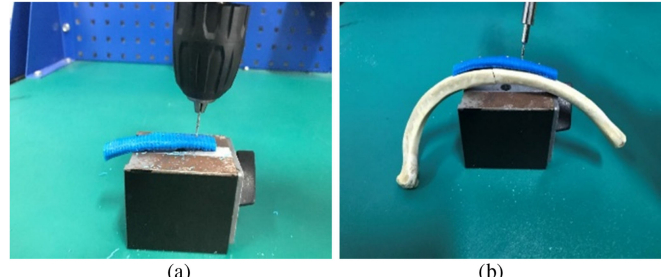


**Fig. 19.** Internal fixation surgery procedure simulation. (a) Drilling holes into the personalized fixation plate and broken bones. (b) Fixing the personalized fixation plate and broken bones using screws.

Referencing the validation strategy in [30] and using the printed personalized plate, we simulated the internal fixation surgery procedure. First, we drilled holes into the personalized fixation plate and the broken bones and fixed them by screws (as shown in Fig. 19). The results of the 3D printing validation are shown in Fig. 20. Notably, the results show that the plates can effectively fix the real fractured ribs. Therefore, the proposed idea to develop personalized internal fixation plates is feasible. Then, to further verify the fixation accuracy, we scanned the entire object (broken bones with personalized fixation plate) using a 3D scanner again and obtained a “postoperative” entire 3D model (as shown in Fig. 21). Next, the original model (before fracture) and the “postoperative” model with the fixation plate were nested and registered. One end of these two models was kept fixed and aligned. Finally, we selected two reference cross-sections respectively at the fracture seams and the other end to count the errors (global 3D error, shifting error and torsion error) using the Geomagic Qualify software (version 11) (as shown in Fig. 22). The error results (in Table II) demonstrate that the personalized internal fixation plate obtained by our method can well recover the curved bone’s original status and complete the fracture reduction with high accuracy.

#### D. Computational Efficiency

This research focuses on clinical treatment, and the computational efficiency of the proposed method influences the treatment effect. Therefore, the computational efficiency should be experimentally evaluated. Table III reports the time consumed by each step of the method. The method was implemented on a standard PC (Intel Core i5-7400 3 GHz with 8 GB of memory). The most time-consuming step in the method is ‘rough registration’ because the OPTICS algorithm is applied in this step to cluster the four projection point sets. The OPTICS

algorithm is complex and requires a long computational time. Moreover, the difference is relatively large among several groups, especially in rough registration, because the number of points and the section shape are very different in these groups. A variety of ribs were chosen to provide a more comprehensive verification. Although the time consumption differed for various groups, the total computational time of the method is short, and the efficiency is satisfactory.

## V. DISCUSSION

As a new research topic, computer-assisted bone fracture reduction and surgery planning has achieved continuous improvement over the past 10 years. In addition to the published literature highlighting the challenges and new trends [5], several (but not very many) relevant methods were also proposed [6]–[11], [15]–[17]. These methods are based on contralateral bone models, statistical shape models or fracture surface characteristics. Such new ideas may be well applied in clinical treatments and receive favorable comments from surgeons. However, these methods are not suitable for curved bone fracture reduction. To our knowledge, no similar study regarding minimally invasive curved bone fracture surgery has been reported, and there are few published studies related to this research issue. A detailed technical computation process regarding how to achieve automatic alignment of curved broken bones (registration) has not been proposed.

Although our framework can provide technical support for computer-aided minimally invasive curved bone fracture surgery, minimally invasive treatment methods still face many challenges. One of the greatest limitations is the hardware system. No specific machine is available for real-time spot

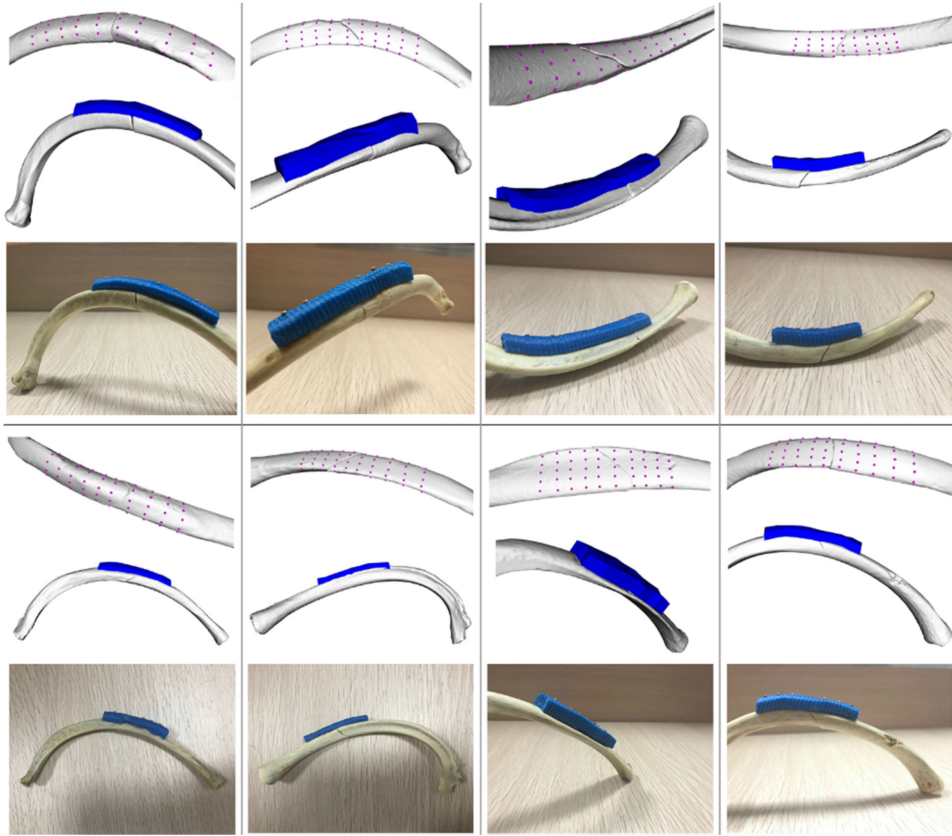


**Fig. 20.** Results of 3-D printing validation. The plates were manufactured using a 3-D printer. A fixation test was performed based on the printed plates and real fractured ribs.

manufacturing of internal fixation plates based on the 3D models obtained from proposed software systems. Another limitation is the absence of novel operation methods. Moreover, the method commonly used to treat fractures is extremely popular and established. Minimally invasive surgical procedures will certainly juxtapose traditional operation methods. There is also a potential issue that may have impact on our method's accuracy. If some tissue at seams is lost and the tissue is large (especially in a real fracture), whether we can obtain an accurate registration result should be a concern. We consider that some manual assistance may be needed.

In the future, we plan to collaborate with electrical engineers and mechanical engineers to design and develop special equipment to automatically and rapidly forge metal internal fixation plates. Additionally, we will further communicate with orthopedists to develop new surgical methods for personalized minimally invasive curved bone fracture surgery.

The present study considers broken bone models obtained from a 3D optical scanner. However, in real clinical treatment, 3D broken models should be reconstructed from computed tomography (CT) or magnetic resonance imaging (MRI) images. Therefore, the feasibility of this procedure must be demonstrated. The quality of the geometric models obtained using these imaging methods and the time required to obtain the models also need to be tested. In the future, we will dedicate more efforts to this issue, and we aim to achieve seam-



**Fig. 21.** “Postoperative” entire 3-D model (broken bones with personalized fixation plate) collection using the 3D scanner.

less transformation from CT/MRI images to 3D broken bone models.

Another issue is how to utilize other imaging methods to acquire 3D bone data in cases where CT is unavailable. The most commonly used method for acquiring bone data is X-rays. In general, we can reconstruct a bone model using a minimum of two directional X-ray images. Under this condition, an X-ray image-based preprocessing method to reconstruct broken bone models should be introduced.

Moreover, this framework focuses on curved bone fractures. Our previously reported framework [16] is applicable for long straight bone fractures. In the future, these two frameworks could be integrated.

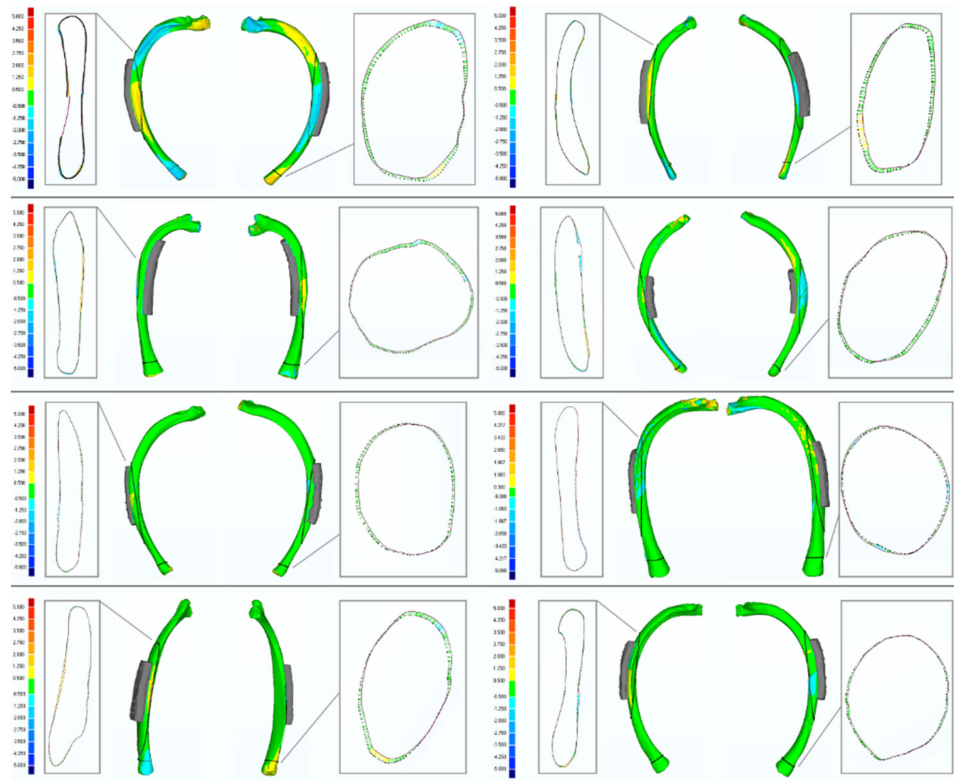


Fig. 22. Geometrical errors (shifting and torsion) on two reference cross-sections (fracture seams and the other end of ribs).

TABLE II  
SHIFTING AND TORSION ERRORS AT THE FRACTURE SEAMS AND THE OTHER END OF RIBS

Index Error	Model_1	Model_2	Model_3	Model_4	Model_5	Model_6	Model_7	Model_8
Global 3D mean/maximum error (mm)	0.504 /2.282	0.311 /1.978	0.361 /1.463	0.436 /1.589	0.226 /1.260	0.353 /2.184	0.292 /1.994	0.326 /1.647
Shifting mean/maximum error of section at fracture seam (mm)	0.380 /1.124	0.317 /0.872	0.348 /0.804	0.418 /1.242	0.275 /0.761	0.245 /0.466	0.378 /0.993	0.300 /0.783
Shifting mean/maximum error of section at the other rib end (mm)	0.411 /1.183	0.321 /0.967	0.238 /0.533	0.324 /0.493	0.260 /0.427	0.075 /0.320	0.323 /0.863	0.159 /0.268
Torsion error of section at the other rib end (°)	0.792	0.440	0.371	0.614	0.077	0.672	0.015	0.654

TABLE III  
TIME CONSUMPTION OF MODEL STEPS (UNIT: s)

Steps	Model_1	Model_2	Model_3	Model_4	Model_5	Model_6	Model_7	Model_8
Curve fitting	0.078	0.062	0.082	0.067	0.066	0.075	0.080	0.076
Capsule projection model construction	1.783	1.402	1.915	1.326	1.598	2.097	2.325	2.064
Rough registration	39.569	58.217	97.583	36.951	27.612	98.504	86.175	92.142
Extraction of cross-section points	1.219	0.214	7.132	0.690	4.777	2.382	22.809	1.939
Precise registration	0.476	0.563	2.337	0.787	1.779	1.324	1.952	0.944
Plate construction	0.005	0.007	0.005	0.005	0.005	0.007	0.005	0.005
Total	43.130	60.465	109.054	39.826	35.837	104.389	113.346	97.170

## VI. CONCLUSION

Many researchers have focused on developing minimally invasive, accurate and personalized surgical schemes to treat bone fractures. To repair curved bone fractures, which frequently occur, we designed an automatic personalized internal fixation plate modeling framework for minimally invasive curved bone fracture surgery based on preregistration with a capsule projection model. In this framework, PCA-K-means-based curve (ridge line) construction, capsule projection model-based feature information extraction, OPTICS-based rough registration and ICP-based accurate registration are utilized for personalized internal fixation plate modeling. By using the designed software, an accurate and personalized internal fixation plate model can be developed according to the curved bone shape of the patient. This framework is shown to be reasonable and feasible in experiments using broken sheep ribs based on three validation experiments (visual validation, computational validation and 3D printing validation). If special equipment is available for metal plate forging in the future, surgeons could provide minimally invasive, accurate and personalized treatment for curved bone fractures.

## ACKNOWLEDGMENT

The authors would like to thank Mrs. X. Peng and Mr. Y. Liu for providing the experimental bones. The authors declare that there are no conflicts of interest related to this paper. The authors declare that they have no financial and personal relationships with other people or organizations that could inappropriately influence their work. All procedures performed in studies involving human participants were in accordance with the ethical standards of the institutional and/or national research committee and with the 1964 Declaration of Helsinki and its later amendments or comparable ethical standards. Informed consent was obtained from all individual participants included in the study.

## REFERENCES

- [1] S. M. Perren, "Physical and biological aspects of fracture healing with special reference to internal fixation," *Clin. Orthopaedics Related Res.*, vol. 68, no. 138, pp. 175–196, 1979.
- [2] P. M. Rommens *et al.*, "Clinical pathways for fragility fractures of the pelvic ring: Personal experience and review of the literature," *J. Orthopaedic Sci.*, vol. 20, no. 1, pp. 1–11, 2015.
- [3] A. Praemer *et al.*, *Musculoskeletal Conditions in the United States*. Rosemont, IL, USA: AAOS, 1999.
- [4] M. E. Müller *et al.*, *Manual of Internal Fixation: Techniques Recommended by the AO-ASIF Group*. New York, NY, USA: Springer, 1991.
- [5] J. J. Jiménez-Delgado *et al.*, "Computer assisted preoperative planning of bone fracture reduction: Simulation techniques and new trends," *Med. Image Anal.*, vol. 30, pp. 30–45, 2016.
- [6] T. Okada *et al.*, "Computer-assisted preoperative planning for reduction of proximal femoral fracture using 3-D-CT data," *IEEE Trans. Biomed. Eng.*, vol. 56, no. 3, pp. 749–759, Mar. 2009.
- [7] T. Albrecht and T. Vetter, *Automatic Fracture Reduction*. Berlin, Germany: Springer, 2012, pp. 22–29.
- [8] R. T. Bicknell *et al.*, "Early experience with computer-assisted shoulder hemiarthroplasty for fractures of the proximal humerus: development of a novel technique and an in vitro comparison with traditional methods," *J. Shoulder Elbow Surgery*, vol. 16, no. 3, pp. S117–S125, 2007.
- [9] P. Fürnstahl *et al.*, "Computer reconstruction of complex proximal humerus fractures for preoperative planning," *Med. Image Anal.*, vol. 16, no. 3, pp. 704–720, 2012.
- [10] M. H. Moghari and P. Abolmaesumi, "Global registration of multiple bone fragments using statistical atlas models: Feasibility experiments," in *Proc. 30th Annu. Int. Conf. IEEE Eng. Med. Biol. Soc.*, 2008, pp. 5374–5377.
- [11] L. Vlachopoulos *et al.*, "Computer algorithms for three-dimensional measurement of humeral anatomy: Analysis of 140 paired humeri," *J. Shoulder Elbow Surgery*, vol. 25, no. 2, pp. e38–e48, 2016.
- [12] S. J. Ulijaszek and C. N. Mascie-Taylor, *Anthropometry: The Individual and the Population*. Cambridge, U.K.: Cambridge Univ. Press, 2005.
- [13] H. Normelli *et al.*, "The length and ash weight of the ribs of normal and scoliotic persons," *Spine*, vol. 10, no. 6, pp. 590–592, 1985.
- [14] F. Zhu *et al.*, "Rib length asymmetry in thoracic adolescent idiopathic scoliosis: Is it primary or secondary?," *Eur. Spine J.*, vol. 20, no. 2, pp. 254–259, 2011.
- [15] L. Vlachopoulos *et al.*, "A scale-space curvature matching algorithm for the reconstruction of complex proximal humeral fractures," *Med. Image Anal.*, vol. 43, pp. 142–156, 2018.
- [16] B. Liu *et al.*, "An automatic personalized internal fixation plate modeling framework for minimally invasive long bone fracture surgery based on pre-registration with maximum common subgraph strategy," *Comput.-Aided Des.*, vol. 107, pp. 1–11, 2019.
- [17] A. S. Chowdhury *et al.*, "Virtual multi-fracture craniofacial reconstruction using computer vision and graph matching," *Comput. Med. Imag. Graph.*, vol. 33, no. 5, pp. 333–342, 2009.
- [18] T. A. Damron *et al.*, "CT-based structural rigidity analysis is more accurate than Mirels scoring for fracture prediction in metastatic femoral lesions," *Clin. Orthopaedics Related Res.*, vol. 474, no. 3, pp. 643–651, 2016.
- [19] G. M. Treccce *et al.*, "Predicting hip fracture type with cortical bone mapping (CBM) in the osteoporotic fractures in men (MrOS) study," *J. Bone Mineral Res.*, vol. 30, no. 11, pp. 2067–2077, 2015.
- [20] A. Nazarian *et al.*, "Treatment planning and fracture prediction in patients with skeletal metastasis with CT-based rigidity analysis," *Clin. Cancer Res.*, vol. 21, pp. 2514–2519, 2015.
- [21] W. D. Leslie *et al.*, "Fracture prediction from repeat BMD measurements in clinical practice," *Osteoporosis Int.*, vol. 27, no. 1, pp. 203–210, 2016.
- [22] Y. Pauchard *et al.*, "Interactive graph-cut segmentation for fast creation of finite element models from clinical ct data for hip fracture prediction," *Comput. Methods Biomed. Eng.*, vol. 19, no. 16, pp. 1693–1703, 2016.
- [23] G. Farin, *Curves and Surfaces for Computer-Aided Geometric Design: A Practical Guide*. Amsterdam, The Netherlands: Elsevier, 2014.
- [24] M. Ankerst *et al.*, "OPTICS: Ordering points to identify the clustering structure," *ACM SIGMOD Rec.*, vol. 28, no. 2, pp. 49–60, 1999.
- [25] P. J. Besl and N. D. McKay, "A method for registration of 3-D shapes," *IEEE Trans. Pattern Anal. Mach. Intell.*, vol. 14, no. 2, pp. 239–256, Feb. 1992.
- [26] D. F. Rogers, *An Introduction to NURBS: With Historical Perspective*. Amsterdam, The Netherlands: Elsevier, 2000.
- [27] P. Fürnstahl *et al.*, *Surgical Treatment of Long-bone Deformities: 3D Pre-operative Planning and Patient-Specific Instrumentation*. Cham, Switzerland: Springer, 2016, pp. 123–149.
- [28] T. Murase *et al.*, "Three-dimensional corrective osteotomy of malunited fractures of the upper extremity with use of a computer simulation system," *J. Bone Joint Surgery, Amer. Volume*, vol. 90, no. 11, pp. 2375–2389, 2008.
- [29] L. Vlachopoulos *et al.*, "Three-dimensional corrective osteotomies of complex malunited humeral fractures using patient-specific guides," *J. Shoulder Elbow Surgery*, vol. 25, no. 12, pp. 2040–2047, 2016.
- [30] S. Omori *et al.*, "Three-dimensional corrective osteotomy using a patient-specific osteotomy guide and bone plate based on a computer simulation system: accuracy analysis in a cadaver study," *Int. J. Med. Robot. Comput. Assisted Surgery*, vol. 10, no. 2, pp. 196–202, 2014.